Chinese Chemical Letters 33 (2022) 793–797

Contents lists available at ScienceDirect

Chinese Chemical Letters

journal homepage: www.elsevier.com/locate/cclet

An endoplasmic reticulum-targeted organic photothermal agent for enhanced cancer therapy

Kaiye Wang[1], Yanan Xiang[1], Wei Pan, Hongyu Wang*, Na Li*, Bo Tang*

College of Chemistry, Chemical Engineering and Materials Science, Key Laboratory of Molecular and Nano Probes, Ministry of Education, Collaborative Innovation Centre of Functionalized Probes for Chemical Imaging in Universities of Shandong, Institute of Molecular and Nano Science, Shandong Normal University, Ji'nan 250014, China

ARTICLE INFO

Article history:
Received 15 May 2021
Revised 17 August 2021
Accepted 18 August 2021
Available online 21 August 2021

Keywords:
Photothermal therapy
Endoplasmic reticulum
Dual-targeting delivery
Organic photothermal agents
Therapeutic agents

ABSTRACT

Developing selectively targeted photothermal agents to reduce side effects in photothermal therapy remains a great challenge. Inspired by the key role of endoplasmic reticulum in the protein synthesis and intracellular signal transduction, particularly for the immunogenic cell death induced by endoplasmic reticulum stress, we developed an endoplasmic reticulum-targeted organic photothermal agent (Ts-PT-RGD) for enhancing photothermal therapy of tumor. The photothermal agent was covalently attached with 4-methylbenzenesulfonamide and cyclic Arg-Gly-Asp (cRGD) peptide for realizing the targeting of endoplasmic reticulum and tumor cell. Owing to its amphiphilic properties, it readily self-assembles in water to form nanoparticles. The photothermal agent possesses excellent photophysical properties and biological compatibility. *In vitro* and *in vivo* experiments demonstrate that it can actively target endoplasmic reticulum and effectively ablate tumor with near-infrared laser.

Selective tumor targeting for reducing damage to normal tissue and efficiently realizing tumor ablation have always occupied the central topic in the cancer therapy [1-4]. Compared to conventional chemotherapy, radiotherapy and surgery, phototherapy including photodynamic therapy (PDT) and photothermal therapy (PTT) possesses inherent advantages of high specificity, minimum invasiveness and negligible drug resistance [5-8], which can directly act on the tumor tissues upon irradiation using near-infrared (NIR) laser. To date, great advances have been made on the development of novel photosensitizers. However, many studies have illustrated that PDT suffered from some drawbacks such as off-target sensitizing effects and irreversible oxidative damage to normal tissues [9]. Meanwhile, it needs an adequate tumor oxygen supply, which limits its applications in hypoxic environments. In view of the above problems, PTT has emerged as a potential safe alternative, because it just demands light and photothermal agent for killing cancer cells *via* converting light energy into hyperthermia [10]. A great number of photothermal materials, including organic and inorganic photothermal agents, have been developed for anticancer therapy [11,12]. But, high intensity irradiation and poor tumor aggregation in the PTT could also damage surrounding normal tissues [13]. It is highly desirable to design and synthesize novel photothermal agent to overcome these challenging problems.

Recently, organelle-targeted PTT of cancer has attracted extensive attention because of its enhanced therapeutic efficacy [14,15]. Particularly for the organic molecule-based photothermal materials, they can be easily and covalently functionalized with organelle-targeted units, which showed excellent biological compatibility and tumor inhibition efficacy [16]. For example, in considering of the susceptibility of mitochondria to temperature, Kim and co-workers pioneered a cryptocyanine dye bearing a triarylphosphonium cation for targeting mitochondrial in order to enhance photothermal therapeutics using NIR laser irradiation [17]. Considerable efforts have also been devoted on the investigations of nuclear-targeting organic photothermal agents because of the thermolabile structure of nuclear matrix [18]. Although much attention has been paid on the mitochondria or nuclear targeted PTT, few advances have been made on the investigation of endoplasmic reticulum (ER)-targeted organic photothermal agent. As we all know, ER as an important organelle plays crucial roles in the protein synthesis, intracellular signal transduction and calcium homeostasis [19]. In addition, it has the largest surface area in cell, which is advantageous for the influx rates of theranostic materials [20]. Furthermore, immunogenic cell death can be induced by ER stress *via* activating intracellular signaling pathways [21-

* Corresponding authors.
E-mail addresses: whongyu@mail.ustc.edu.cn (H. Wang), lina@sdnu.edu.cn (N. Li), tangb@sdnu.edu.cn (B. Tang).
[1] These authors contributed equally to this work.

https://doi.org/10.1016/j.cclet.2021.08.087
1001-8417/

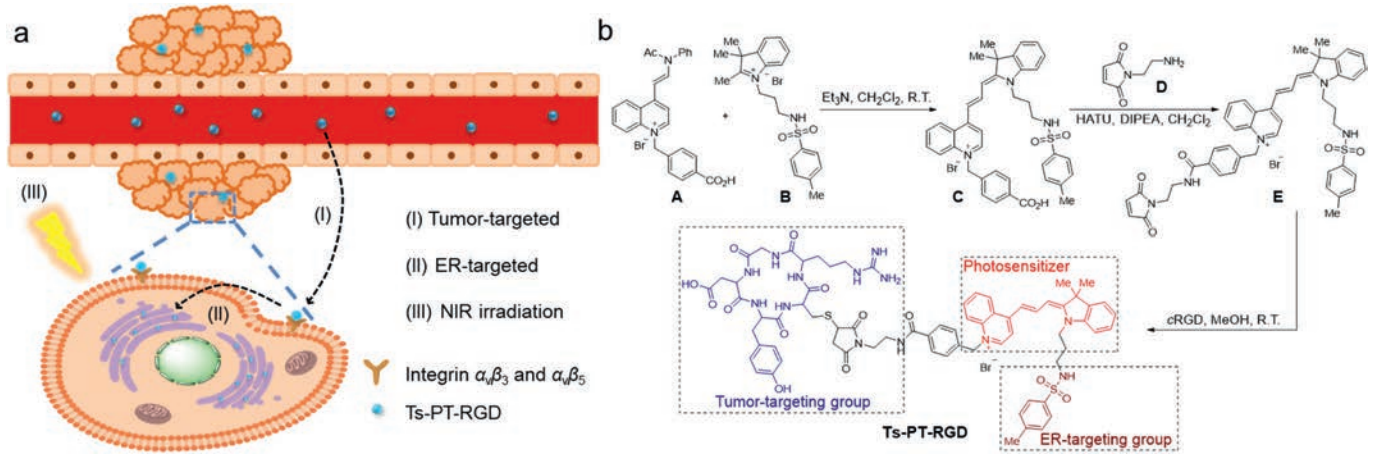

Scheme 1. (a) The target and treatment principle of Ts-PT-RGD. (b) Synthesis of Ts-PT-RGD. HATU: 2-(7-aza-1*H*-benzotriazole-1-yl)-1,1,3,3-tetramethyluronium hexafluorophosphate; DIPEA: *N*,*N*-diisopropylethylamine.

23]. Notably, You and co-workers recently reported an ER-targeting gold nanosphere combing with PDT/PTT for enhancing immunogenic cancer cell death [21]. Therefore, ER has been recognized as an ideal target for developing organelle-targeted cancer treatment [24]. To our knowledge, ER-targeted PTT based on organic photothermal agent still remains unexplored.

Our group has always focused on the development of efficient theranostic agents for cancer therapy, including the design of organic and inorganic photosensitive materials [25-28]. In particular, we have been interested in the active-targeting cancer therapy, which is favorable for enhancing therapeutic efficacy and reducing damages to the normal tissues [27,28]. In this pursuit, we herein decided to develop an ER-targeted organic photothermal agent, which could be selectively delivered to cancer cells *via* active-targeting system (Scheme 1a). Recent studies have shown that cRGD peptide possesses excellent biological compatibility and hydrophilicity *in vivo*, which functionalizes as a targeting ligand of integrins $\alpha_v\beta_3$ and $\alpha_v\beta_5$ [29,30]. Due to the superior properties of cRGD, it was then selected for realizing the goal of specifically targeting cancer cell membranes. In addition, for targeting ER, 4-methylbenzenesulfonamide (Ts) was selected because of its outstanding targeting ability [31,32]. Hemicyanine dye (PT) was selected as the main part of dual-targeted photothermal agent for heat generation [27].

The ER-targeted photothermal agent (Ts-PT-RGD) was firstly prepared *via* simple operations from readily available materials (Scheme 1b). It could be directly purified by high performance liquid chromatography (HPLC). The detailed synthesis steps and characterizations of the compound were shown in Supporting information (Scheme S1, Figs. S1-S3). Subsequently, we explored the physical properties of Ts-PT-RGD including its hydrophilicity and diameter. To our delight, this photothermal agent as an amphiphilic compound could self-assemble in water to form well dispersed spherical nanoparticles (average diameter, 75 nm) (Fig. 1a). The dynamic light scattering experiment showed that the diameter of Ts-PT-RGD was mostly distributed in 122 ± 15 nm, and Ts-PT-RGD possessed good stability (Figs. S6 and S7 in Supporting information). After that, the photophysical properties of Ts-PT-RGD were also investigated. Fig. 1b showed that the maximum absorption of Ts-PT-RGD was 610 nm, and its fluorescence emission was 651 nm (Fig. S9a in Supporting information). The time-dependent temperature changes of Ts-PT-RGD (0.5 mmol/L) at different power densities were also explored under irradiation of 635 nm laser (Fig. 1c). The temperature increased higher as increasing the power density of laser

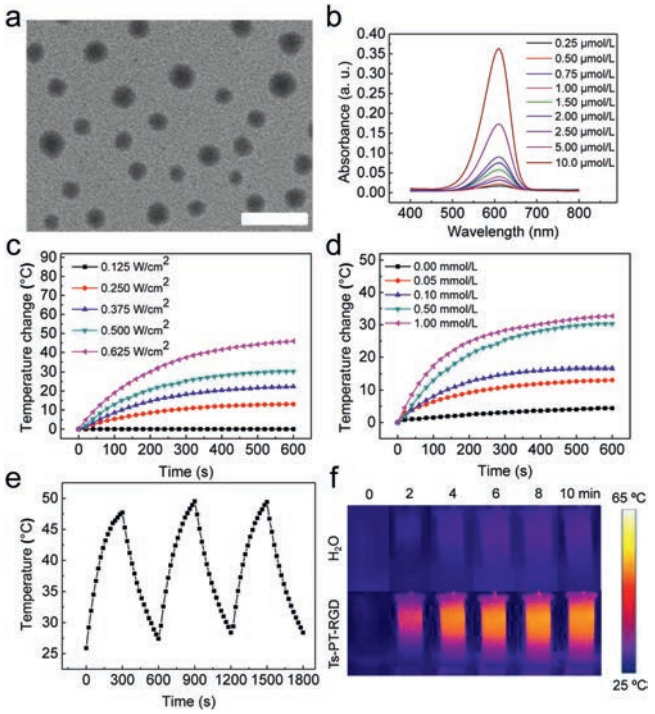

Fig 1. (a) Transmission electron microscope image of Ts-PT-RGD nanoparticles. Scale bar is 200 nm. (b) UV-vis absorption spectra of Ts-PT-RGD with different concentrations. (c) Time-dependent temperature changes of Ts-PT-RGD (0.5 mmol/L) at different power densities under irradiation of 635 nm laser. (d) Time-dependent temperature changes of Ts-PT-RGD at different concentrations under irradiation of 635 nm laser (0.5 W/cm^2). (e) Temperature cycling curves of Ts-PT-RGD (0.5 mmol/L) over three on-off cycles of 635 nm laser (0.5 W/cm^2) irradiation. (f) Thermal images of Ts-PT-RGD (0.5 mmol/L) under 635 nm laser (0.5 W/cm^2) irradiation for 10 min.

at the same time, and the temperature could increase by 30.3 °C when the power density was 0.5 W/cm^2. In view of the safety of the adjacent normal tissues, the irradiation intensity was chosen at 0.5 W/cm^2. Subsequent examination of the effect of concentration of Ts-PT-RGD under irradiation of 635 nm (0.5 W/cm^2) revealed the best choice at 0.5 mmol/L for PTT (Fig. 1d). According to the method reported by Yang *et al.*, the photothermal conversion efficiency of Ts-PT-RGD was calculated as 38.91% (Fig. S10 in Supporting information). Furthermore, temperature cycling curves experi-

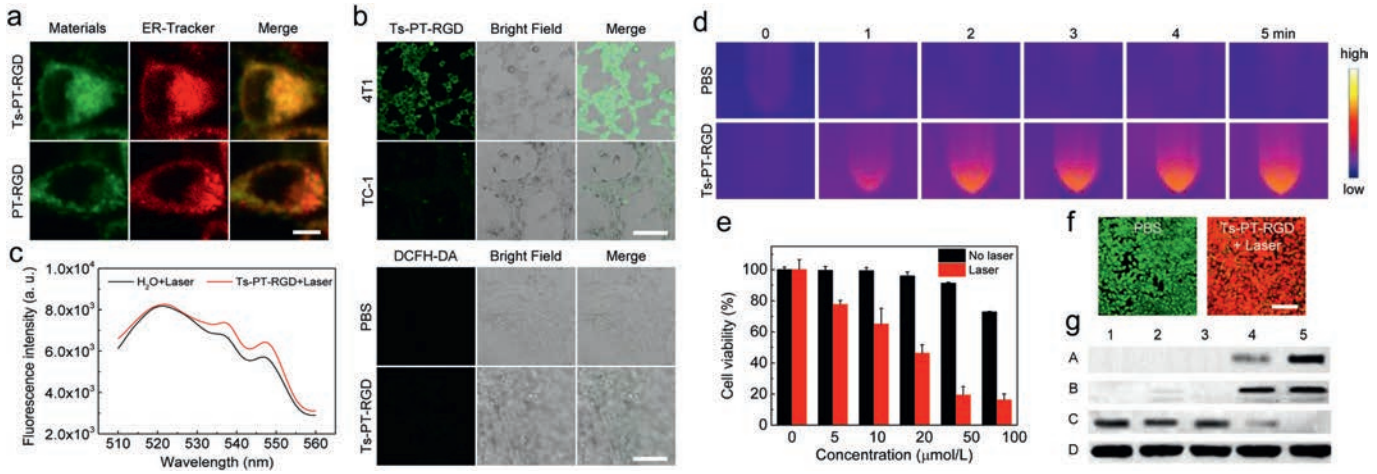

Fig 2. (a) The location of Ts-PT-RGD and PT-RGD with ER. Scale bar is 7.5 μm. (b) CLSM images of 4T1 and TC-1 cells treated with Ts-PT-RGD. Scale bar is 100 μm. (c) The fluorescence intensity of 2′,7′-dichlorofluorescin diacetate (DCFH) solutions with different treatments. And CLSM images of 4T1 cells treated under different conditions to evaluate ROS production based on Reactive Oxygen Species Assay Kit (DCFH-DA) fluorescence intensity. Scale bar is 100 μm. (d) Thermal image of 4T1 cells incubated with Ts-PT-RGD (50 μmol/L) or PBS under 635 nm laser irradiation (0.5 W/cm^2) for 5 min. (e) MTT assays of 4T1 cells with different concentrations of Ts-PT-RGD with or without laser (n = 3). (f) Live/dead cell staining assays of 4T1 cells with different treatments. Scale bar is 100 μm. (g) Western blot analysis of caspase-3 and CHOP proteins expressed in 4T1 cells after treatment with 1 (PBS), 2 (Laser), 3 (Ts-PT-RGD, 50 μmol/L), 4 (PT-RGD+Laser, 50 μmol/L), and 5 (Ts-PT-RGD+Laser, 50 μmol/L) for 8 h. A: CHOP; B: Cleaved-caspase-3; C: Pro-caspase-3; D: GAPDH. Laser power: 0.5 W/cm^2, 5 min.

ments showed that Ts-PT-RGD still exhibited excellent photothermal conversion efficiency after three on-off cycles (Fig. 1e). Under 635 nm laser irradiation for 10 min, Ts-PT-RGD (0.5 mmol/L) had a significant temperature increase compared with water (Fig. 1f). In addition, no significant change in fluorescence intensity was observed within 30 min, which suggested that the photostability of Ts-PT-RGD fulfilled the requirement of the subsequent cancer therapy (Fig. S9b in Supporting information).

Next, *in vitro* antitumor effect of Ts-PT-RGD was further investigated under irradiation of 635 nm (0.5 W/cm^2). To evaluate the ER-targeting ability of Ts-PT-RGD, cells were firstly incubated with Ts-PT-RGD or PT-RGD under the same culture conditions, and then ER was stained with ER-tracker red to perform subcellular localization experiments. As shown in Fig. 2a and Fig. S11 (Supporting information), Ts-PT-RGD overlapped well with ER-tracker red, while PT-RGD failed to overlap with it. Meanwhile, immunofluorescence staining also confirmed the same results (Fig. S12 in Supporting information). Subsequently, the endoplasmic reticulum fluorescence assay showed that the fluorescence intensity of the Ts-PT-RGD group was 12.4 times that of the PT-RGD group (Fig. S13 in Supporting information). All results indicated that the Ts moiety of Ts-PT-RGD played crucial role in targeting ER. The cancer-targeting ability of Ts-PT-RGD was examined by the cellular uptake behavior of 4T1 or TC-1 cells (Fig. 2b). The fluorescence intensity of 4T1 cells was significantly higher than that of TC-1 cells, indicating that Ts-PT-RGD was more inclined to be internalized by cancer cells than normal cells, which also elaborated the ability of Ts-PT-RGD to target cancer cells. In addition, DCFH and DCFH-DA were used to illustrate the ability of Ts-PT-RGD to generate reactive oxygen species in aqueous solution and cells respectively (Fig. 2c). These results showed that no noticeable reactive oxygen species were generated using Ts-PT-RGD. So it also suggested that PDT and oxygen have little effect on the cytotoxicity. Subsequently, the temperature change of the cells after incubation with Ts-PT-RGD before and after laser irradiation was investigated. As shown in Fig. 2d, Ts-PT-RGD exhibited excellent photothermal effect *in vitro*. The cytotoxicity of different concentrations of Ts-PT-RGD with or without laser irradiation were continued to be examined in order to investigate the biocompatibility of materials. No significant damage to the cells were observed when Ts-PT-RGD was used in the range of 0-50 μmol/L without laser irradiation. When the cells were incubated with 50 μmol/L Ts-PT-RGD, the cell viability was higher than 90% without laser irradiation. Contrarily, the cell viability was less than 20% upon NIR laser irradiation (Fig. 2e). Meanwhile, the cell-killing ability of PT-RGD was also examined. As shown in Fig. S14 (Supporting information), PT-RGD could kill tumor cells after laser irradiation, but the killing ability of PT-RGD was lower than that of Ts-PT-RGD under the same experimental conditions. After that, the cytotoxicity of Ts-PT-RGD (50 μmol/L) was also confirmed by live/dead cell staining assays (Fig. 2f and Fig. S15 in Supporting information). Control experiments including PBS, laser and Ts-PT-RGD groups showed no obvious cell damages. Moreover, Ts-PT-RGD had better cell killing ability than PT-RGD under the same conditions. Based on the previous works [33], we proposed that ER stress induced by PTT activated intracellular signaling pathways to promote immunogenic cell death. To get preliminary insights of the mechanism of ER-targeting PTT, western blot experiments were performed to detect apoptotic signaling molecules (Fig. 2g). Previous research suggests that CHOP (C/EBP-homologous protein) as an important apoptotic signaling molecule in the apoptosis pathway could be activated by ER stress [34], so we subsequently explored the CHOP expression of cells *via* Western blot experiments at different conditions. No changes were detected when cells were treated with PBS, laser and Ts-PT-RGD, but the CHOP expression of cells incubated with Ts-PT-RGD plus laser group was significantly increased. Especially, it is higher than PT-RGD plus laser group. Mitochondrial apoptotic proteins casepase-3 was also investigated in this process, and Ts-PT-RGD plus laser group also exhibited the highest cleaved-caspase-3 expression. All the results suggested that ER-targeting PTT could induce more severe ER stress, and these apoptotic signaling molecules could promote cancer cell apoptosis (uncropped scants of western blots were presented in Fig. S16 in Supporting information).

To verify the antitumor efficacy of Ts-PT-RGD *in vivo*, active targeting ability of Ts-PT-RGD for cancer therapy was firstly explored through fluorescence imaging. As shown in Fig. 3a, 6 h after the intravenous injection of Ts-PT-RGD in mice, the fluorescence in tumor was significantly higher than that in other sites, indicating that Ts-PT-RGD had excellent tumor targeting ability. As the fluorescent intensity of the tumor intravenously injected with Ts-PT-

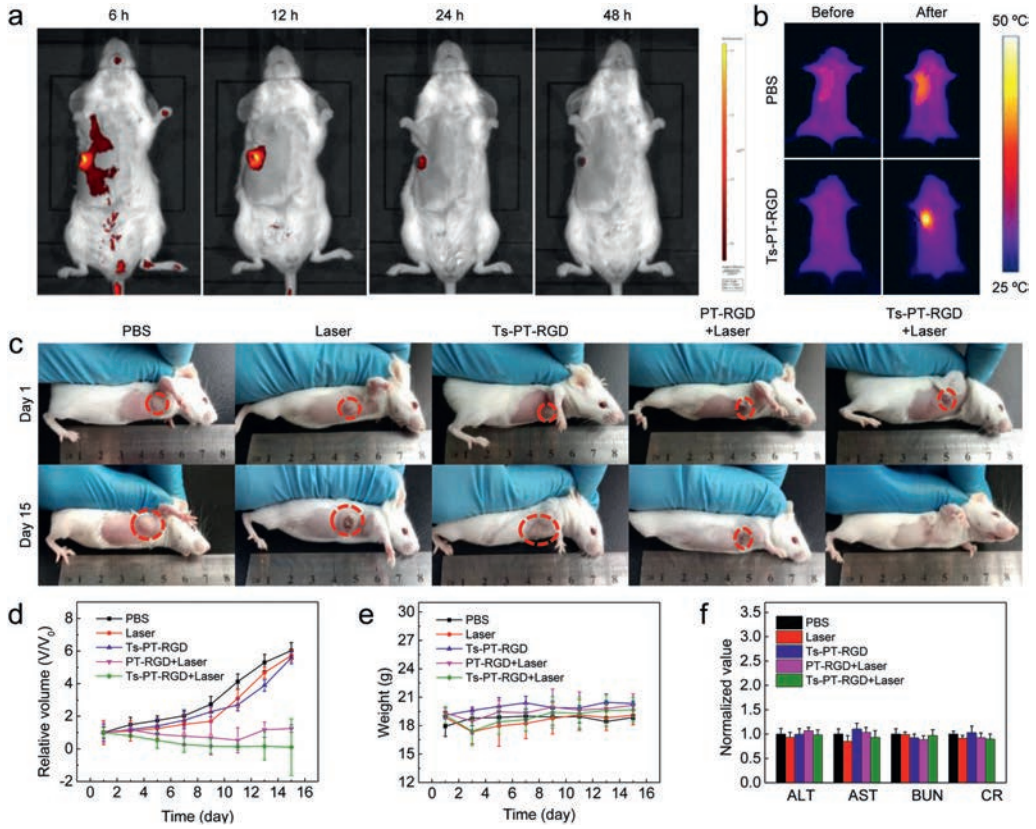

Fig 3. (a) Fluorescence imaging at different time points of 4T1 tumor bearing mice after intravenous injection of Ts-PT-RGD (0.5 mmol/L). (b) Thermal images of 4T1 tumor bearing mice after intravenous injection of Ts-PT-RGD (0.5 mmol/L) or PBS under 635 nm laser (0.5 W/cm^2) irradiation for 10 min. (c) Pictures of different groups mice on day 1/15 after different treatments. (d) Relative tumor volume curves, (e) Body weight change curves and (f) blood biochemistry analysis of different groups mice after different treatments (n = 3). ALT: alanine aminotransfease; AST: aspartate aminotransferase; BUN: blood urea nitrogen; CR: creatinine

RGD reached a maximum after 12 h (Fig. S17 in Supporting information), the laser irradiation was initiated for PTT after 12 h in subsequent experiments. We found that the fluorescence intensity of Ts-PT-RGD in the mouse was disappeared after 48 h, so the material could be metabolized well in the body without long-term toxicity. In particular, fluorescence imaging of major organs and tumors at different time points also confirmed these results (Fig. S18 in Supporting information). Thermal imaging *in vivo* illustrated that the maximum temperature was higher than 46 °C *via* laser irradiation for 10 min after intravenously injected with Ts-PT-RGD, so it also confirmed that Ts-PT-RGD was suitable for cancer therapy (Fig. 3b). To test the tumor inhibition effect of Ts-PT-RGD, 4T1 tumor-bearing mice were randomly divided into five groups and intravenously injected with different materials at the same time. The relative tumor volume of group 1 (PBS), group 2 (Laser) and group 3 (Ts-PT-RGD) grew rapidly without inhibitory effect, thus suggesting that Ts-PT-RGD possesses low biotoxicity. Although group 4 (PT-RGD+Laser) showed obvious tumor inhibition ability at first, tumor recurrence was observed at the later stage of treatment. Only group 5 (Ts-PT-RGD+Laser) exhibited excellent suppression, and the tumor almost disappeared at last *via* PTT. These results indicated that the ER- and tumor-targeting PTT had superior therapeutic effect, importantly, it could effectively prevent tumor recurrence (Figs. 3c and d). *In vivo* PTT with Ts-PT-RGD significantly improved the survival rate of 4T1 tumor-bearing mice. All mice in the Ts-PT-RGD+Laser group survived for more than 35 days, while all of the control groups died within 25 days (Fig. S19 in Supporting information). In addition, there were no significant changes in body weight of mice in each group during treatment (Fig. 3e).

Finally, to explore biosafety and side effects of the photothermal agent, hematoxylin and eosin (H&E) staining slices of heart, liver, spleen, lung and kidney were carefully assessed after 7 days of treatment. Meanwhile, the injury of the tumor was tested after 12 h (Fig. S20 in Supporting information). No significant necrosis or injury were found in the main organs of the five groups of mice, while the tumors of mice intravenously injected with PT-RGD and Ts-PT-RGD had obvious damage under laser irradiation. Especially, the tumor of mice intravenously injected with Ts-PT-RGD showed the greatest damage under laser irradiation. In addition, the blood biochemistry was tested (Fig. 3f). Data for each indicator did not differ significantly between the different treatment groups. All the results suggested that Ts-PT-RGD was a biosafety photothermal agent.

In conclusion, a novel ER-targeted organic photothermal agent for selective anti-tumor therapy was successfully developed. The organic photothermal agent readily self-assembles in water to form nanoparticles owing to its excellent amphiphilic properties, and it also displayed high photothermal conversion efficiency and photostability for cancer therapy. *In vitro* experiments indicated that Ts-PT-RGD possessed excellent ER-targeting ability and enhanced the therapeutic efficacy. *In vivo* experiments illustrated that the ER-targeted organic photothermal agent exhibited better tumor inhibitory effect than the photothermal agent without ER-targeted ligand. Preliminary investigations on the expression of CHOP and caspase-3 of cells illustrated that ER stress induced by ER-targeting PTT could promote cancer cell apoptosis. We anticipate that the ER-targeted strategy can provide new avenues for ER-based therapeutic agents and further development of PTT.

Ethical statement

All animal procedures were performed in accordance with the Principles of Laboratory Animal Care (People's Republic of China) and were approved by the Animal Care and Use Committee of Shandong Normal University (Ji'nan, China).

Declaration of competing interest

The authors declare that they have no known competing financial interests or personal relationships that could have appeared to influence the work reported in this paper.

Acknowledgments

This work was supported by National Natural Science Foundation of China (Nos. 21927811, 21874086 and 21775094), National Key R&D Program of China (No. 2019YFA0210100), and Youth Innovation Science and Technology Program of Higher Education Institution of Shandong Province (No. 2019KJC022).

Supplementary materials

Supplementary material associated with this article can be found, in the online version, at doi:10.1016/j.cclet.2021.08.087.

References

[1] C. Liang, L.G. Xu, G.S. Song, et al., Chem. Soc. Rev. 45 (2016) 6250–6269.
[2] J.J. Li, A. Dirisala, Z.S. Ge, et al., Angew. Chem. Int. Ed. 56 (2017) 14025–14030.
[3] L.M. Pan, J.N. Liu, J.L. Shi, Chem. Soc. Rev. 47 (2018) 6930–6946.
[4] Z.Z. Yu, W. Pan, N. Li, et al., Chem. Sci. 7 (2016) 4237–4244.
[5] Y.J. Liu, P. Bhattarai, Z.F. Dai, et al., Chem. Soc. Rev. 48 (2019) 2053–2108.
[6] S.S. Lucky, K.C. Soo, Y. Zhang, Chem. Rev. 115 (2015) 1990–2042.
[7] Z.J. Cheng, T. Zhang, W.L. Wang, et al., Chin. Chem. Lett. 32 (2021) 1580–1585.
[8] D.P. Chen, Z.H. Zhong, Q.L. Ma, et al., ACS Appl. Mater. Interfaces 12 (2020) 26914–26925.
[9] Z.J. Zhou, J.B. Song, L.M. Nie, et al., Chem. Soc. Rev. 45 (2016) 6597–6626.
[10] J.Q. Chen, C.Y. Ning, Z.N. Zhou, et al., Prog. Mater. Sci. 99 (2019) 1–26.
[11] S. Liu, X.T. Pan, H.Y. Liu, Angew. Chem. Int. Ed. 59 (2020) 5890–5900.
[12] H.S. Jung, P. Verwilst, A. Sharma, et al., Chem. Soc. Rev. 47 (2018) 2280–2297.
[13] K.Y. Wang, Y.N. Xiang, W. Pan, et al., Chem. Sci. 11 (2020) 8055–8072.
[14] W.H. Chen, G.F. Luo, X.Z. Zhang, Adv. Mater. 31 (2019) 1802725.
[15] P. Gao, W. Pan, N. Li, et al., ACS Appl. Mater. Interfaces 11 (2019) 26529–26558.
[16] X.J. Song, Q. Chen, Z. Liu, Nano Res. 8 (2015) 340–354.
[17] H.S. Jung, J.H. Lee, K. Kim, et al., J. Am. Chem. Soc. 139 (2017) 9972–9978.
[18] G.Y. Wan, Y.Y. Cheng, J. Song, et al., Chem. Eng. J. 380 (2020) 122458.
[19] Y. Wen, C.L. Schreiber, B.D. Smith, Bioconjugate Chem. 31 (2020) 474–482.
[20] J.M. Meinig, L.Q. Fu, B.R. Peterson, Angew. Chem. Int. Ed. 54 (2015) 9696–9699.
[21] W. Li, J. Yang, L.H. Luo, et al., Nat. Commun. 10 (2019) 3349.
[22] K.B. Huang, F.Y. Wang, H.W. Feng, et al., Chem. Commun. 55 (2019) 13066–13069.
[23] Y.H. Li, X.H. Liu, W. Pan, et al., Chem. Commun. 56 (2020) 1389–1392.
[24] Z.Q.Q. Feng, H.M. Wang, S.Y. Wang, et al., J. Am. Chem. Soc. 140 (2018) 9566–9573.
[25] N. Li, Q.Q. Sun, Z.Z. Yu, et al., ACS Nano 12 (2018) 5197–5206.
[26] Z.Z. Yu, Y.G. Ge, Q.Q. Sun, et al., Chem. Sci. 9 (2018) 3563–3569.
[27] H.Y. Wang, J.J. Chang, M.W. Shi, et al., Angew. Chem. Int. Ed. 58 (2019) 1057–1061.
[28] H.Y. Wang, J.J. Chang, W. Pan, et al., Nanoscale 11 (2019) 18021–18025.
[29] J.X. Chen, H.Y. Wang, C. Li, et al., Biomaterials 32 (2011) 1678–1684.
[30] F.G. Giancotti, E. Ruoslahti, Science 285 (1999) 1028–1033.
[31] H.B. Xiao, P. Li, X.F. Hu, et al., Chem. Sci. 7 (2016) 6153–6159.
[32] S. Xu, H.W. Liu, X.X. Hu, et al., Anal. Chem. 89 (2017) 7641–7648.
[33] X. Xu, S. Gupta, W.L. Hu, et al., PloS One 6 (2011) e23740.
[34] R. Sano, J.C. Reed, Biochim. Biophys. Acta 1833 (2013) 3460–3470.